Linking Atmospheric Rivers, extreme precipitation and river discharge in the Rhine catchment

Jeroen Sonnemans

Supervisors:

Imme Benedict

Albrecht Weerts

A thesis submitted in partial fulfilment of the degree of Master of Science

at Wageningen University and Research Centre,

The Netherlands.

March 17, 2021

Wageningen, The Netherlands

WAGENINGEN

UNIVERSITY & RESEARCH

1 Abstract

Globally, river floods have become more frequent and are expected to occur more often in the future. Main driver is the intensification of the hydrological cycle and the accessory increase of landward water transport in the form of Atmospheric Rivers (ARs). In previous studies, ARs were mostly linked with extreme precipitation in coastal areas. However, in this study we investigated the link between ARs, extreme precipitation and floods for a region located more inland, the Rhine catchment. First, we found a significant increase of AR occurrence and intensity from 1950-2020. We detected less ARs in the Alps, and discussed the role of the applied AR-detection method. Moreover, we show a strong sensitivity of discharge peaks to water storage preceding extreme precipitation events. As a rapid follow-up of events results in a high build-up of water storage in the form of groundwater or snow, we recommend to study the link between consecutive events and discharge peaks further.

Contents

2 Introduction

Over the last decades, floods have become more frequent globally (Blöschl et al., 2015) and the amount of river floods in Europe will increase even more in the future (Alfieri et al., 2015). Climate change contributes strongly to this as it intensifies the hydrological cycle (Allan et al., 2014; Lavers et al., 2013; Hill et al., 2018). To be prepared against river floods, it is key to understand the processes of large-scale moist transport in the atmosphere that may lead to extreme precipitation regionally and thus to floods (Ionita et al., 2020). When looking at the mid-latitudes, water is mainly transported in the form of Atmospheric Rivers (ARs) (Guan and Waliser, 2019).

ARs are long narrow zones of vertically integrated water transport from low to high latitudes (Rutz et al., 2014). About 75% of the water transport in ARs takes place in the lowest 2,25 km of the atmosphere (Ralph and Dettinger, 2012). Most of the time, about 3-5 ARs are present worldwide (Guan and Waliser, 2019) and these are responsible for more than 90% of the total water transport in the midlatitudes (Ralph and Dettinger, 2012; Rutz et al., 2014). On average, precipitation from ARs contributes to 22% of the river discharge globally (Paltan et al., 2017).

ARs are often associated with extratropical cyclones (Ralph and Dettinger, 2012), but Stohl et al. (2008) also showed an extreme rainfall event caused by an AR with (sub)tropical source. With Lagrangian moisture tracking, they were able to find water transport over 40 degrees latitude. Guan and Waliser (2019) applied moisture tracking algorithms to show that ARs originate mostly at the western boundaries of oceans and rain out on the eastern boundaries. Because of this mechanism, west-coast areas generally receive the largest amounts of rain by ARs.

As a result, ARs can supply high amounts of precipitation in Norway and California, sometimes resulting in floods. Both areas are located on western continental margins with high mountain ranges along it, which are sensitive to AR landfall and orographic precipitation enhancement (Benedict et al., 2019; Stohl et al., 2008). ARs are also a major source of extreme rainfall events at many other locations in Europe, for example in Portugal and Spain (Ramos et al., 2015), UK (Lavers et al., 2011) and France (Lu et al., 2013). In general, ARs reach further inland in western Europe than in the western United States, because the Rocky Mountains constrain inward flows of ARs along the coast of West America (Gimeno et al., 2016). During winter the share of ARs in (extreme) precipitation in Europe is relatively large, leading to many floods, but summer floods are mainly caused by convective precipitation (Gimeno et al., 2016; Ionita et al., 2020).

Regarding ARs, an interesting area inland of Europe is the catchment of the Rhine , which is one of Europe's largest rivers and its most important inland water way (Ionita et al., 2020). The catchment is a densely populated area and is of strong economic importance (Ionita et al., 2020). Next to that, potential flood damage is estimated to be around 300 billion € for the total basin (Te Linde et al., 2011). Therefore research on the occurrence of ARs in the Rhine catchment and the coherent flood risks is relevant.

The link between ARs and floods is already demonstrated in the study by Ionita et al. (2020), who linked the 10 largest floods of the lower Rhine basin in the last 100 years with the occurrence of an atmospheric river. In this research, the link between ARs, extreme precipitation and discharge in the Rhine basin is further investigated. ARs generally supply more rain in mountainous regions, because of orographic enhancement of precipitation (Stohl et al., 2008). Therefore, this study compares the Upper-Rhine (the Alps) with the Lower Rhine catchment (lowland) in the experiments. Where Ionita et al. (2020) use discharge observations, we will apply a hydrological model here to test the sensitivity of discharge to the initial conditions.

Because climate change increases the frequency and magnitude of ARs globally (Allan et al., 2014; Lavers et al., 2013), our study aims to show if frequency and magnitude of ARs change over the years in the Rhine catchment. Furthermore, this studies focusses on the link between ARs and extreme precipitation. Lastly, we zoom in on the influence of conditions preceding ARs on the height of the discharge peaks. The research questions are:

What is the link between ARs, extreme precipitation and discharge in the Rhine catchment?

1. How do the frequency and intensity of ARs in the Rhine catchment vary over years and within the region?
2. What is the relation between ARs and (extreme) precipitation events in the Upper and Lower Rhine catchment?
3. What is the influence of groundwater and snow preceding an AR on river discharge in the Upper and Lower Rhine?

3 Data & Methods

First, the applied datasets in this study are described in section 3.1. In section 3.2, the method of detecting Atmospheric Rivers (ARs) is explained. As a following step, the procedure of linking detected ARs with extreme precipitation is described in chapter 3.3. The discharge simulation and model validation are explained in section 3.4. Lastly, the sensitivity analysis of discharge to the initial groundwater storage and snow depth is described in chapter 3.5.

3.1 Data

To detect ARs, ERA5 hourly data with horizontal wind and specific humidity on multiple pressure levels from 1950 to 2020 was used (Hersbach et al., 2020). ERA5 has a higher spatial and temporal resolution than ERA-Interim with a horizontal resolution of 0.25°x0.25° and a vertical range from 1000 hPa - 1 hPa with global coverage. For this research, only data from October till March is included. Two grids with different configurations were applied as shown in table 1 and figure 1:

- The region indicated as “AR-detection area” was selected to detect Atmospheric Rivers (ARs). The Atlantic basin was included here, since ARs mostly originate from this region (Benedict et al., 2019; Ionita et al., 2020). The specific humidity (q) and horizontal wind components (u and v) were extracted at all available pressure levels. To reduce the duration of the calculations, the resolution for this grid was manually lowered to 1°x1°.
- For the “Rhine catchment” region the same variables as in the AR-detection area grid were selected, but with the full ERA5 resolution of 0.25°x0.25°. Additionally, daily precipitation (P) is extracted for this grid.

Table 1: Overview of ERA5 data used for this study.

Grid	Resolution	Variables	Latitudes	Longitudes
AR-detection area	1°x1°	q, u, v	20°-60°N	70°W-20°E
Rhine catchment	0.25°x0.25°	q, u, v, P	46.5°-52.25° N	4.75°-10.5° E

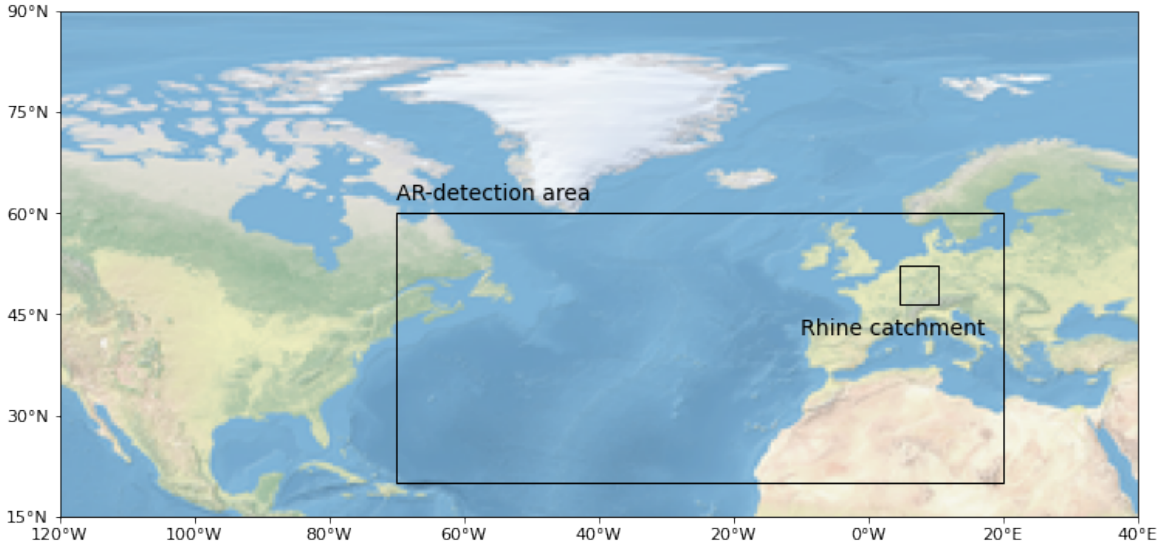

Figure 1: Map showing the "AR-detection area" grid and the “Rhine catchment” in blue. See table 1 for the grid specifications.

Furthermore, a separate ERA5 dataset (1979-2019) was used for the Rhine catchment as forcing data for the hydrological model Wflow_sbm, including precipitation, evaporation and average surface temperature per day. To make the data applicable for the model, the original resolution (0.25°x0.25°) was downscaled to (0.00833°x0.00833°). The more detailed grid points were differentiated with a DEM and the lapse rate, representing the temperature decrease with increasing altitude. More background of the hydrological model is provided in section 3.4.

Lastly, datasets containing daily discharge observation were obtained from GRDC (Global Runoff Data Centre) in order to validate river discharge simulations. The dataset for Basel had a time

range from 1900-2016 and the one for Lobith covered the years 1901-2017. The locations of Basel and Lobith are indicated in figure 3.

3.2 AR-detection

To be able to detect ARs, the Integrated Vapor Transport (IVT) value needs to be **≥250 kg m^{-1} s^{-1} for a contiguous length of ≥2000 km** according to the definition of Rutz et al. (2014). The IVT is defined as

$$IVT = \frac{1}{g} \int_{1000hPa}^{100hPa} q\mathbf{V} dp \tag{1}$$

where g is the gravitational acceleration (m s^{-2}), q is the specific humidity (kg kg^{-1}), $\mathbf{V}$ is the horizontal wind vector (m s^{-1}), consisting of an u and v component and p is the pressure level (hPa). The integration over pressure levels is calculated with 50-hPa intervals ranging from 1000 to 100 hPa.

The length of a zone with IVT ≥ 250 kg m^{-1} s^{-1} can be calculated with the maximum great-circle distance between all combinations of included coordinates. For this, the haversine formula was used

$$d = 2R \arcsin\left(\sqrt{\sin^2\left(\frac{\varphi_1 - \varphi_2}{2}\right) + \cos\varphi_1 \cos\varphi_2 \sin^2\left(\frac{\lambda_2 - \lambda_1}{2}\right)}\right) \tag{2}$$

with R as radius of the earth (km), φ_1 and φ_2 as latitudes of two coordinates (radians), λ_1 and λ_2 as longitudes (radians) of the same two coordinates. The example in figure 2 would be detected as AR, partly overlapping the Rhine catchment.

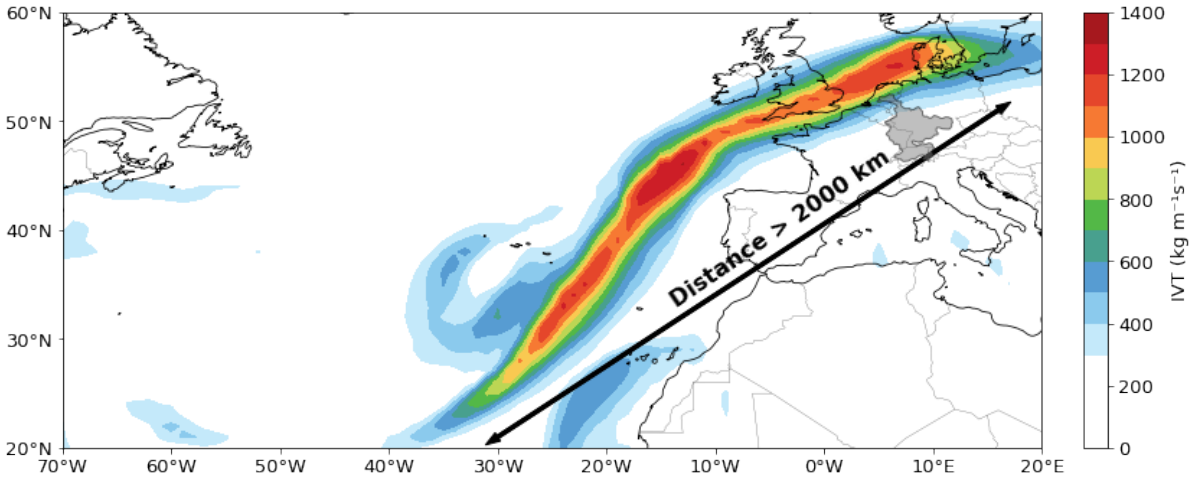

Figure 2: Example of an Atmospheric River on 26 October 2019, partly overlapping the Rhine catchment shown in grey. The colors show the IVT values above 250 kg m^{-1} s^{-1}. The circular IVT contours around (35°N, 30°W) represent hurricane Pablo (KNMI, 2020)

AR detection was performed for the AR-detection area grid (figure 1) on four times per day (0:00, 6:00, 12:00 and 18:00, Central European Time). Consequently, precipitation in the Rhine catchment on a day with a detected AR was classified as AR-related.

3.3 ARs and extreme precipitation

To link the occurrence of ARs with extreme precipitation, a climatology of both had to be constructed first. The temporal variation of AR occurrence and intensity over the years 1950-2020 were investigated and also extreme and total yearly precipitation were analysed. Furthermore, regression lines were used to find a change over years and a slope with a P-value<0.05 was considered to be significant. The spatial variation was investigated by differences per coordinate in the whole Rhine catchment (figure 3).

Secondly, extreme precipitation and ARs were linked separately for the Upper and Lower Rhine catchment. The regions were divided as illustrated in figure 3a, with the most orography in the Upper Rhine catchment (figure 3b). Days exceeding the 90th, 95th and 99th percentiles of daily precipitation were selected for both areas. From those selected days, the AR-related percentage was determined. Next to that, a scatterplot of IVT with extreme precipitation days will be constructed for the coordinates of the red starts in figure 3a,

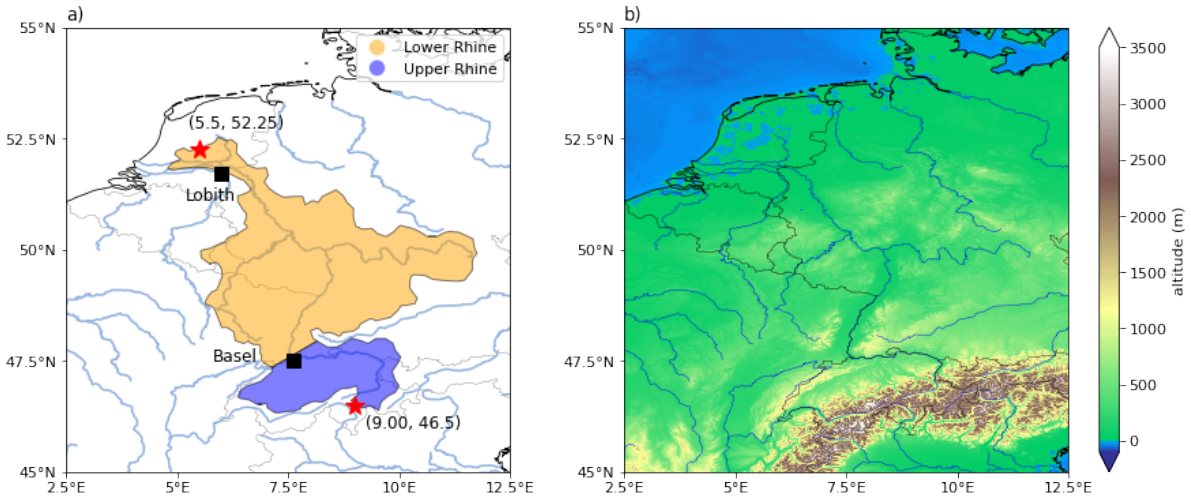

Figure 3: a) A map of the Rhine catchment, divided into the Upper and the Lower Rhine. The black squares are discharge measuring stations of Basel and Lobith. The red stars indicate specific coordinates in the Upper and Lower-Rhine on which IVT and daily extreme precipitation were linked. b) Orography map of the Rhine catchment.

3.4 Hydrological model

In our study, we used a high-resolution conceptual hydrologic model with parameterization for the Rhine catchment, called Wflow_sbm (Imhoff et al., 2020). This simple bucket model (SBM) takes complex soil properties into account without the need of further calibration to be able to

simulate discharge. To run the model, the forcing dataset as described in section 3.1 was used. We simulated river discharge (m^3 s^{-1}) of the Rhine in Basel and Lobith (figure 3a), following after two selected events with extreme precipitation.

The simulated timeseries of 5 months were compared with the observed discharge at both locations and the model performance was rated with a Nash-Sutcliffe Efficiency (NSE) as calculated below with (Cooper, 2010):

$$NSE = 1 - \frac{\sum_{t=1}^{N}[q_{obs} - q_{sim}]^2}{\sum_{t=1}^{N}[q_{obs} - \breve{q}_{obs}]^2} \tag{3}$$

Here N is the length of the time series in days, q_{obs} is the observed discharge, $\breve{q}_{obs}$ is the mean observed discharge of the time series and q_{sim} is the simulated discharge (all in m^3 s^{-1}). When the NSE-value of the model equals 1, the discharge as simulated by Wflow_sbm corresponds completely with the observed discharge. An NSE-value above 0 means that the simulation is a better discharge predictor than the observed mean ($\breve{q}_{obs}$).

3.5 Discharge sensitivity to snow and water storage

For both events, three runs were performed to simulate river discharges in Basel and Lobith with different initial conditions. A first run was executed as base run with the aim to simulate the event as it occurred in reality and lasted for a period of 5 months. Here the initial conditions were determined by running the model with a spin-up time of one year prior to the event. For the other two runs, the initial conditions were slightly altered. The second run contained a snow map with a thicker snow layer on average in the Rhine catchment ("Increased snow run") and the third run had a map with a higher water storage in the soil at the start ("Increased storage run"). These new maps were extracted from time steps in the base run with the highest average groundwater storage and respectively the thickest snow layer. The three runs started one day prior to the event and the differences between the simulated discharge peaks directly after the event were compared.

4 Results

The results consist of a meteorological part followed by a hydrological part. First, the climatology of precipitation and ARs are presented in chapter 4.1 and the relation between both is further explained in section 4.2. The two selected precipitation events that are used for the discharge simulations are shown in chapter 4.3

The hydrology part consists of three chapters (section 4.4 - 4.6). First, the hydrological model wflow_sbm is validated. Next, the differences between the initial conditions of the three runs are shown. Lastly, the resulting discharges of all runs are explained.

4.1 Climatology of precipitation and ARs

Looking at figure 4a, the average precipitation in the winter season (October-March) over the Rhine basin is around 500 mm. With around 800mm precipitation in the Rhine catchment over the whole year (DWD, 2020), the winters are generally wetter than the summers. Also a strong interannual variation was found in the amount of total winter precipitation. Furthermore, the regression line showed an increase over the years, but it was not significant. In figure 4b, we see extreme daily precipitation over the whole Rhine catchment with a 99-percentile close to 15 mm/day, while the median of daily precipitation is only 1.3 mm/day. There was no clear change over the years following the trend line, but again a strong yearly variation was visible.

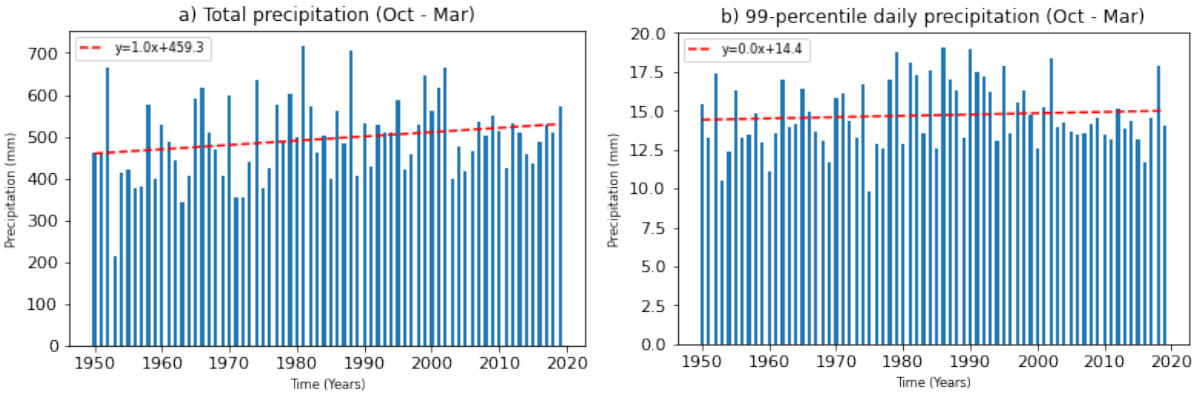

Figure 4: a) Total precipitation (October – March) per year in the Rhine catchment on average. The red dotted line shows the regression line with its formula in the top left and the P-value of the slope was 0.06. b) The 99-percentile of daily precipitation averaged over the Rhine catchment each year (October – March). The yearly trend is indicated in the top left as well.

In contrast with extreme precipitation, we saw a clear significant increase of AR-occurrences in figure 5a. Around 1950, ARs occurred only 16% of time in the Rhine catchment, whereas they occur about 21% of time in 2020. Moreover, the AR intensity also increased significantly over the years following figure 5b. The maximum IVT value of Rhine catchment ARs was on average 860 kg m^{-1} s^{-1} around 1950, but increased to values about 930 kg m^{-1} s^{-1} nowadays. The variation in yearly AR occurrence was relatively strong (figure 5a), but the mean AR intensity did not vary much over the years (figure 5b).

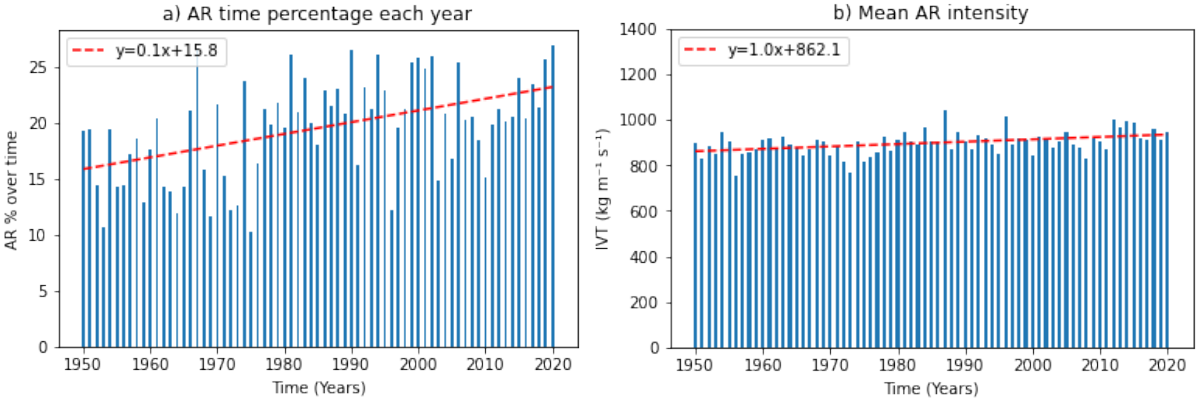

Figure 5: a) Percentage of time steps with AR occurrence over the Rhine catchment per year (October – March). The red dotted line is a regression line with its formula shown above and a P-value of 0.0. b) The mean AR intensity per year (October – March). The AR-intensity is defined by the maximum IVT value reached in the AR. A regression line is visualised by the red dashed line and the P-value of the slope was again 0.0.

Strong spatial differences were found between extreme precipitation amounts (figure 6a). The highest daily extremes were present in the Upper Rhine catchments with 99-percentiles of daily precipitation over 30 millimeters per day. The river valleys in the northern half of the catchment had the least extreme precipitation with values of only 15 millimeters.

In contrast, ARs were most frequently present in the western and northwestern part of the Rhine catchment, about 17 % of time (figure 6b). This frequency decreased gradually to the southeast and in the Alps ARs occured locally only 2% of time steps. The AR-occurrences in figure 6a are lower than the numbers in figure 5a because AR detections over the catchment as a whole are taken into account in figure 5a.

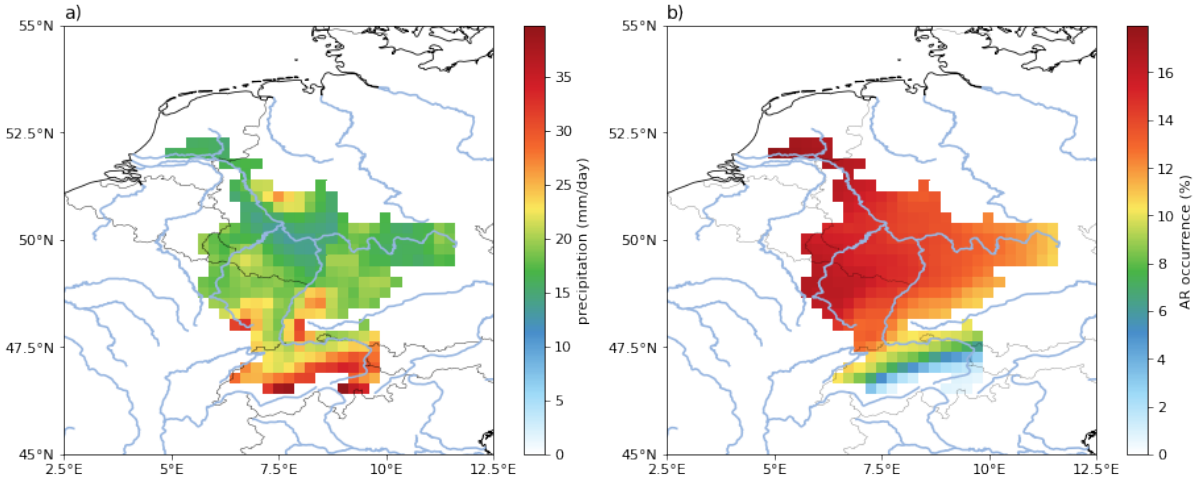

Figure 6: a) The 99-percentile of daily precipitation between 1950-2020. b) Percentage of time steps (4 per day) with AR occurrences in the Rhine catchment per coordinate within the Rhine catchment (1950-2020).

As an AR is defined with a length of at least 2000 km, ARs over the Rhine catchment also cover areas outside of it as illustrated in figure 7. Most ARs over the Rhine catchment overlapped with southwestern regions and about half of the ARs is simultaneously located over the Azores. Approximately 30% of the ARs were even stretched over the 60°W meridian. Despite that, less than 10% of the detected ARs reached areas south of the Alps.

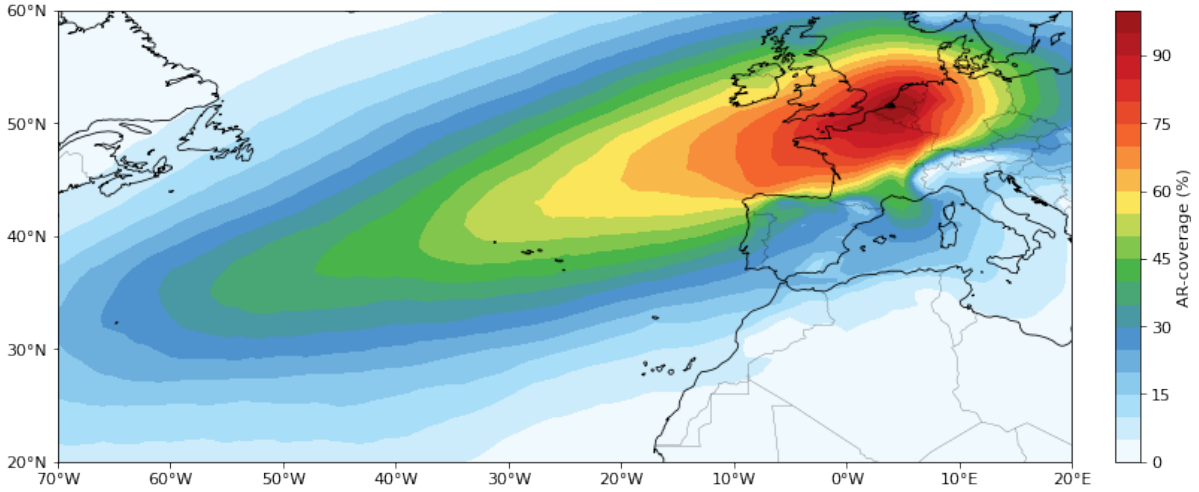

Figure 7: Percentage of all ARs over the Rhine catchment (detection 4 times per day), with the same AR covering each location on the map.

4.2 Linking ARs, IVT and extreme precipitation

The described temporal and spatial variations of precipitation and ARs in chapter 4.1 are connected in this section. The relation between IVT and daily precipitation at two coordinates are shown in figure 8. Both coordinates are visualised on the map of figure 3a. The Lower Rhine coordinate corresponds with the location in figure 6b with the most detected ARs and the Upper Rhine coordinate had the least amount of AR detections in figure 6b.

Despite the low AR-occurrence at the Upper Rhine coordinate, a strong link between daily precipitation and IVT could be observed in figure 8. As IVT values in the Upper Rhine coordinate mostly stay below the 250 kg m^{-1} s^{-1} threshold, ARs were only exceptionally detected there. Higher IVT values were found at the Lower Rhine coordinate, but the link with daily precipitation is less evident here. Moreover, the precipitation extremes at the lower Rhine coordinate were lower than those at the Upper Rhine coordinate in figure 8. This is also in line with the extreme precipitation map of figure 6a.

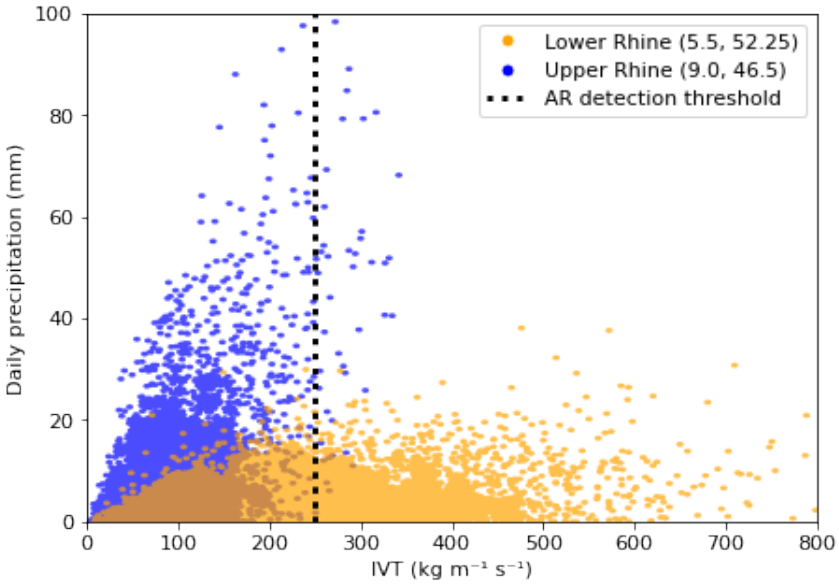

Figure 8: Scatterplot of IVT and precipitation over the years 1950-2020 for a coordinate in the Upper-Rhine and one in the Lower-Rhine (see locations at figure 3a). Each dot shows daily values and the dashed line indicates the IVT threshold for AR-detection of 250 kg m^{-1} s^{-1}. Only 187 out of 12848 days exceeded the threshold at the Upper Rhine coordinate.

A different approach is shown in the barplot of figure 9, where we linked ARs and daily precipitation for two areas instead of two coordinates. A higher fraction of precipitation days was associated with ARs in the Lower Rhine compared to the Upper-Rhine. However, the precipitation values above the bars are higher for the Upper Rhine compared to the Lower Rhine. This confirms the highest extreme precipitation values at the Upper Rhine in figure 8 despite the little amount of detected ARs. Lastly, more precipitation days were related to AR with increasing precipitation thresholds as expected.

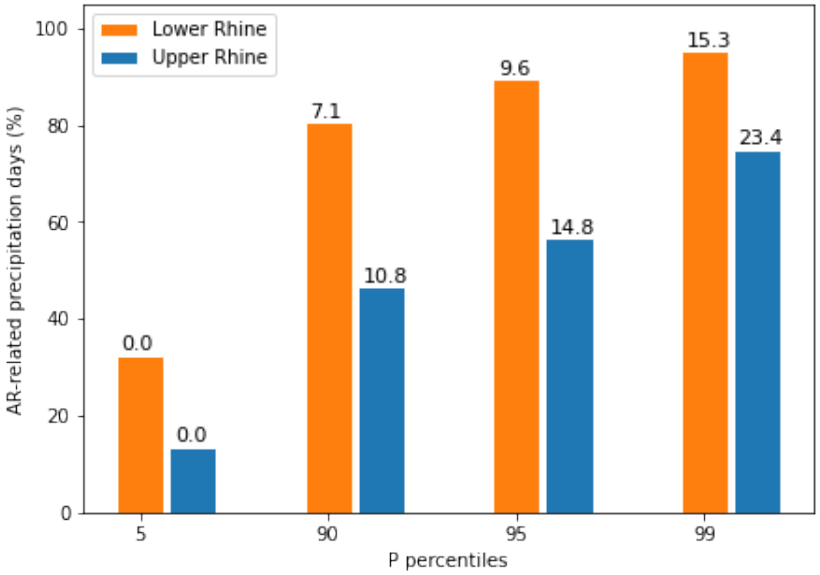

Figure 9: The percentage of days exceeding each precipitation thresholds that was classified as AR-related in the Upper and Lower Rhine catchment. The thresholds are defined by precipitation percentiles in both areas and the belonging precipitation values in millimeters are plotted above each bar. The areas are specified in figure 3.

4.3 Extreme precipitation and discharge

In order to analyse the Rhine discharge after an AR, this study zoomed in at two extreme precipitation events in figure 4. The first event took place over the Upper-Rhine area, whereas a second one was chosen over the Lower-Rhine area close to Lobith as shown in figure 2b. Both events were accompanied by the presence of ARs. In following sections, the results from the hydrological model Wflow_sbm are shared.

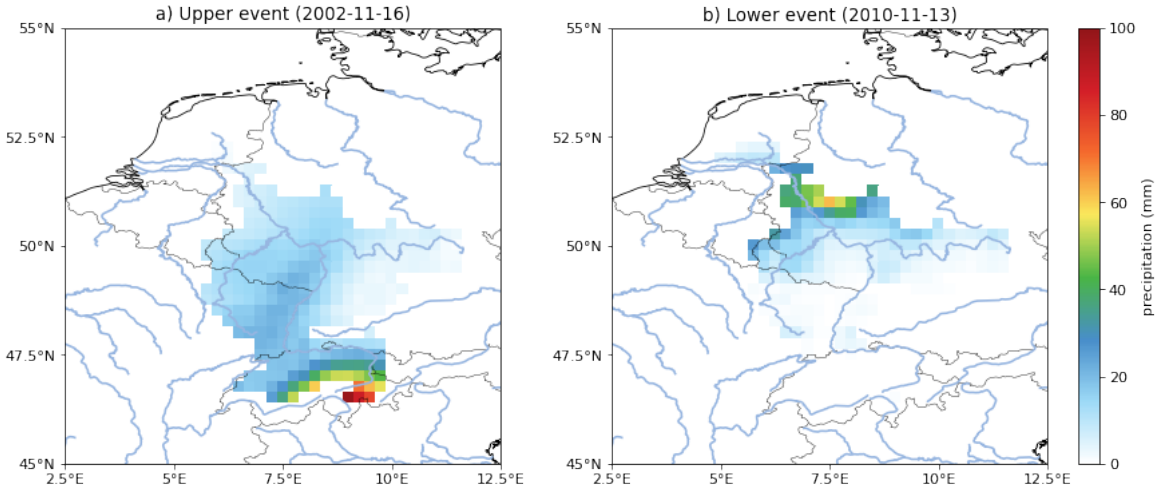

Figure 10: The precipitation event over the Upper-Rhine (2002-11-16) is shown on the left and is referred to as "Upper event". The Lower-Rhine event (2010-11-13) is depicted on the right and is called "Lower event".

4.4 Hydrological model validation

As a first step, the model was validated in this subsection based on the discharge simulations for Basel and Lobith after both precipitation events as shown in figure 11. In Basel (11a,b) the fit was especially good for the first half of the run, but a structural underestimation by the model appeared from February onwards. For Lobith (11b,d) the simulated baseflow corresponded well with the observations, except for an overestimation of some discharge peaks. Despite the deviations, the NSE values of 0.63-0.83 in figure 11 represent a good model performance. An NSE value of 1 would indicate a perfect fit with the observations (see section 3.4). The highest peaks were expected directly after the event, but a few higher peaks were observed in December and January. These were probably the result of subsequent precipitation events.

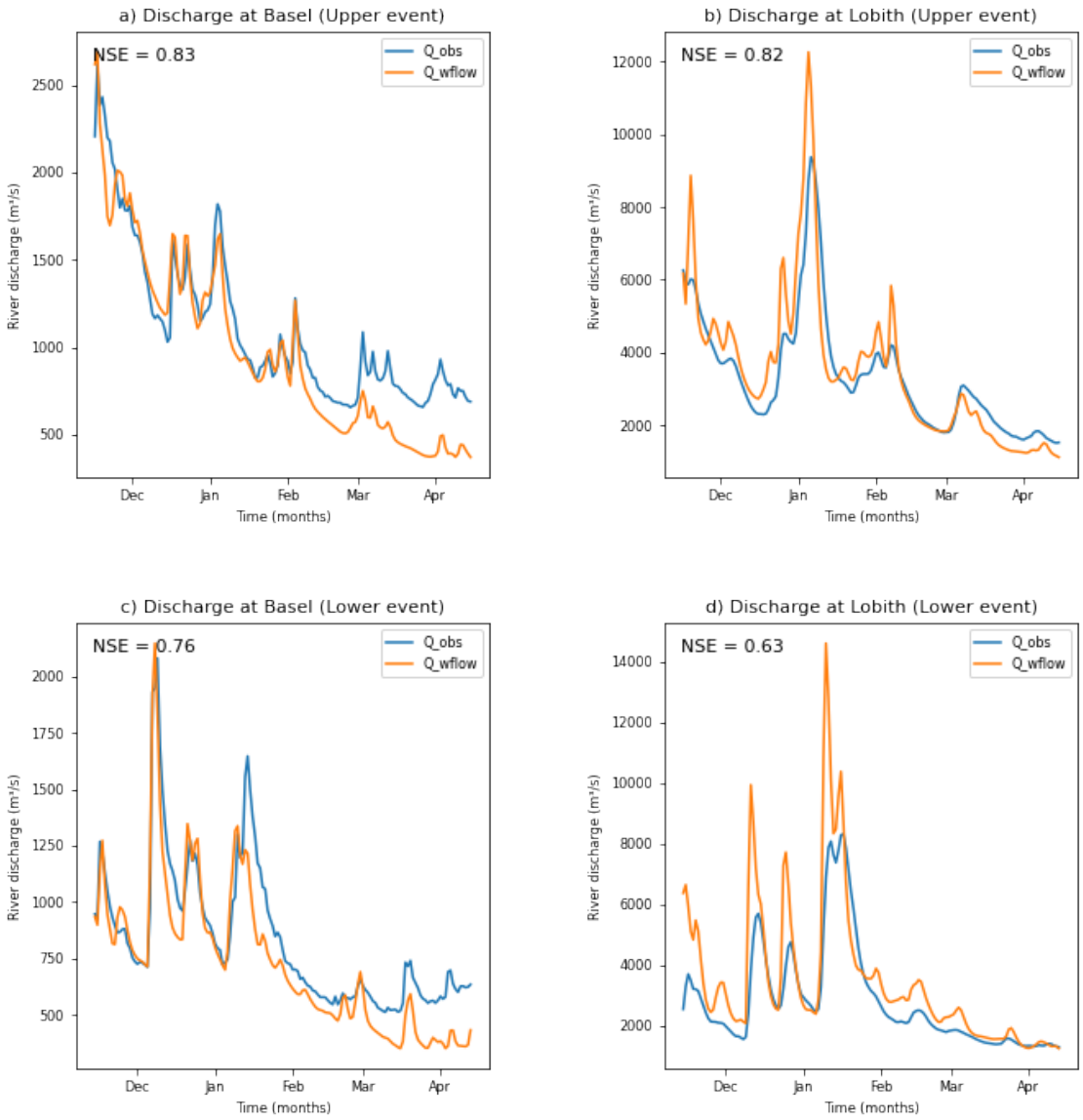

Figure 11: In each graph the simulated discharge (orange) was compared with the observed discharge (blue) and the belonging NSE values are shown. The graphs on the top show the discharge for 5 months after the Upper event (16-11-2002) for Basel and Lobith. On the bottom, the same kind of graphs were constructed for the Lower event (13-22-2010).

Moreover, the model was validated with a discharge simulation from 1979-1989, of which the first year was used as spin-up period. Here we found and NSE of 0.55 in Lobith and 0.66 in Basel. A sufficient model performance was assumed from these values. Imhoff et al. (2020) also validated the model for 2011-2016. They found an NSE of 0.76 in Emmerich, located close to Lobith and 0.27 in Basel. Reason for the higher value in Basel in our study could be the further improved representation of glaciers.

4.5 Preceding snow and groundwater conditions

In this section, the different initial conditions of the three runs as described in section 3.5 are explained. In figure 12, the initial snow and storage maps of the increased snow and storage runs were compared with the standard initial conditions of the base run. For the increased snow runs of both events, the map with the most snow in the base run was used as initial condition instead of the original snow map at the end of the spin-up period. In the Upper event, the increased snow layer was mainly located in the Alps (figure 12a), while the snow addition was more equally distributed over the Rhine catchment in the Lower event (figure 12b).

In the increased storage run, the initial storage map was replaced by the map from the base run with the highest average storage in the catchment. Despite that, some areas had less storage in the high storage map than in the original map, indicated with blue colors (figure 12c,d). For both events, the storage decrease mainly appeared in the Upper Rhine catchment.

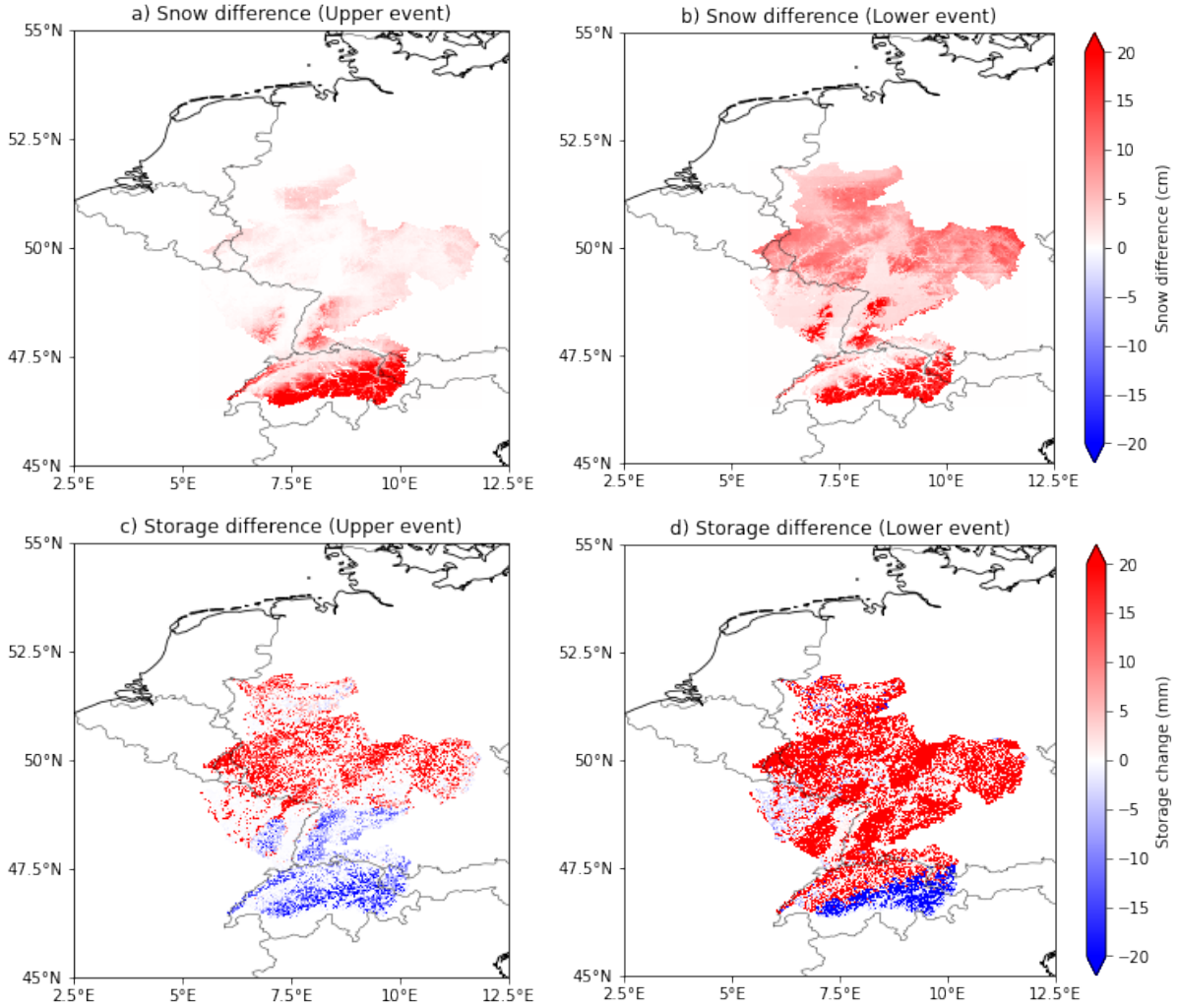

Figure 12: On the left, the initial snow layer map of the increased snow run relative to the base run is depicted. On the right the initial storage map of the increased storage run is compared with the base run. The colourbar boundaries are limited to values between -20 and 20 to make regional differences visible.

4.6 Discharge simulations

When looking at the discharge directly after the event (figure 13 and table 2), we see the highest peaks in the increased snow and storage run as we expected. At the Lower event in Lobith (figure 13d), the peak of the increased storage run was even more than four times higher than the base run with a discharge of more than 30000 m^3 s^{-1} (figure 13d). This is almost twice as high as the discharge level used for designing flood defenses in The Netherlands, which is 16000 m^3 s^{-1} (Te Linde et al., 2011). A simultaneous, but less extreme peak was also found in Basel (figure 13c). After the Upper event, extreme discharge values over 3600 m^3 s^{-1} were simulated in the increased snow run for Basel (figure 13a). These levels have a return period of about 10 years (BAFU, 2017). Logically, the discharge in Lobith was always higher than in Basel, because of its location further upstream in the Rhine catchment.

Unexpected result was the low discharge in the increased storage run compared to the base run of the Upper event in Basel (figure 13a). However, this could be explained by the initial storage map of figure 12b. Compared to the base run, more groundwater was present in the Rhine catchment as whole, but less groundwater was located upstream of Basel, resulting in less discharge there. In Lobith (figure 13b), the discharge peaks of the increased storage run are higher than in the base run.

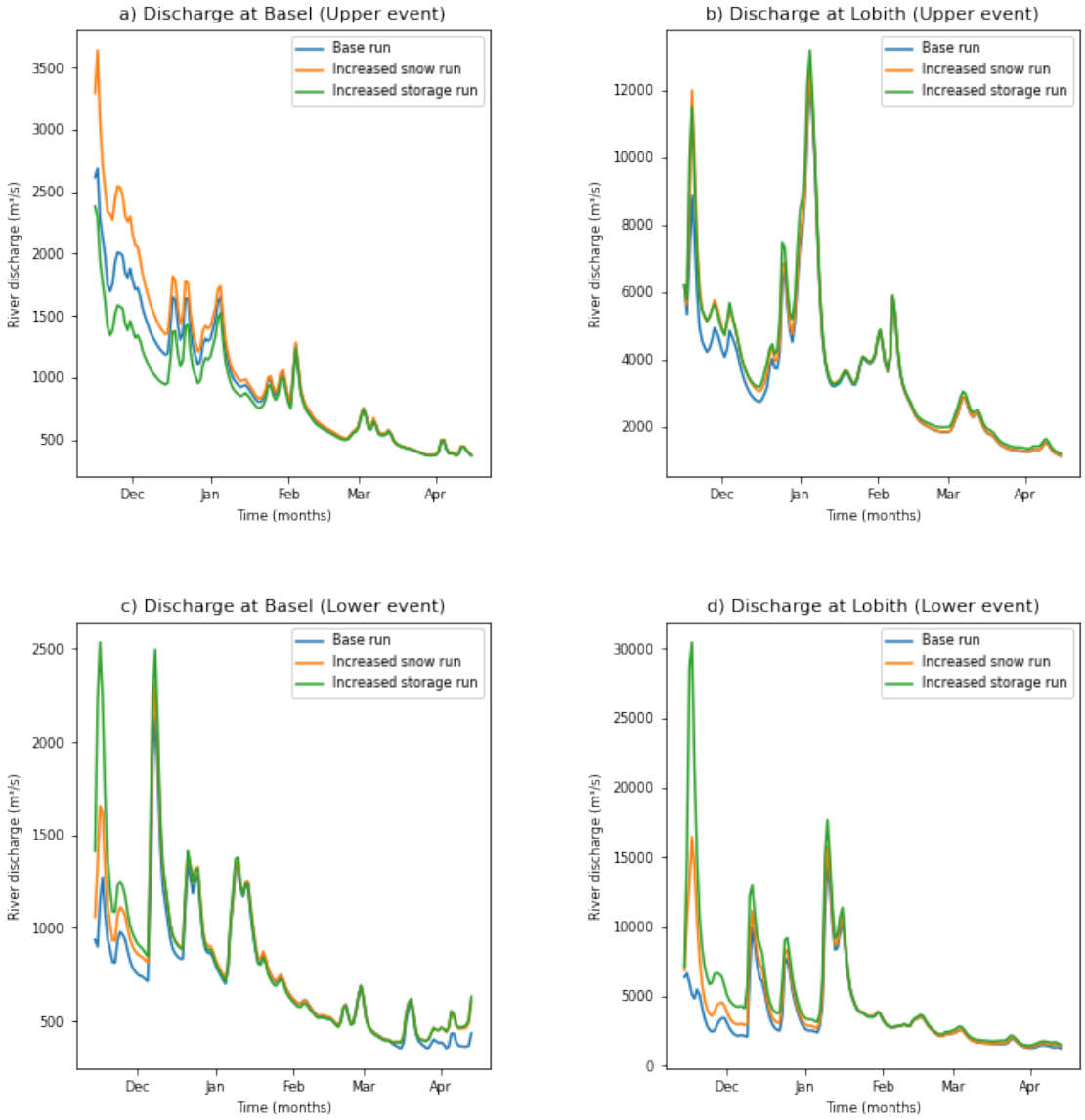

Figure 13: Simulated discharges in Basel and Lobith up to 5 months after the occurrence of the Upper event (15-11-2002) and the Lower event (13-11-2010). The base run simulated the discharge as in reality. The increased snow run contains an initial map with a thicker snow layer and the increased storage run started with a map with more groundwater storage.

Table 2: Peak discharges (m^3 s^{-1}) of the base run, increased snow run and increased storage run directly after the Upper and Lower event in Basel and Lobith.

	Upper event		Lower event	
Run	Basel	Lobith	Basel	Lobith
Base run	2687	8866	1273	6643
Increased snow run	3641	12001	1654	16470
Increased storage run	2379	11508	2535	30450

Figure 14 demonstrated an almost constant difference between the snow layer in the increased snow run and the base run in simulations of both events. However, two exceptions were found. The first one was found during the first days after the events, during which the snow reduced in the increased snow run, but accumulated in the base run. This was in line with figure 15, that showed some snow accumulation in the Alps, but much snow melt outside the Alps for the increased snow run. The snow decrease was not observed in the base runs of figure 14, because less snow was available there to melt. This explains the difference between the discharge peaks of the increased snow run and the base run in figure 13 and table 2. As a second exception, converging lines were visible at the end of the timeseries in the Lower event. The thicker snow layer in the increased snow run resulted in more snow melt in spring compared to the base run.

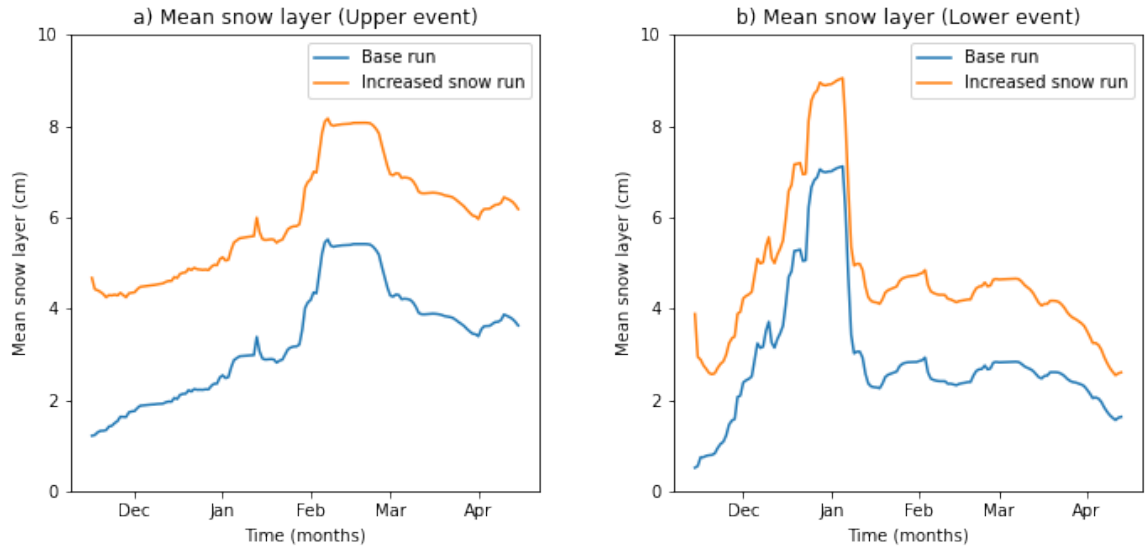

Figure 14: The evolution of the mean snow layer in the Rhine catchment in the base run and the increased snow run for a) The Upper event and b) The Lower event. The increased storage run is not included because the snow is the same as in the base run.

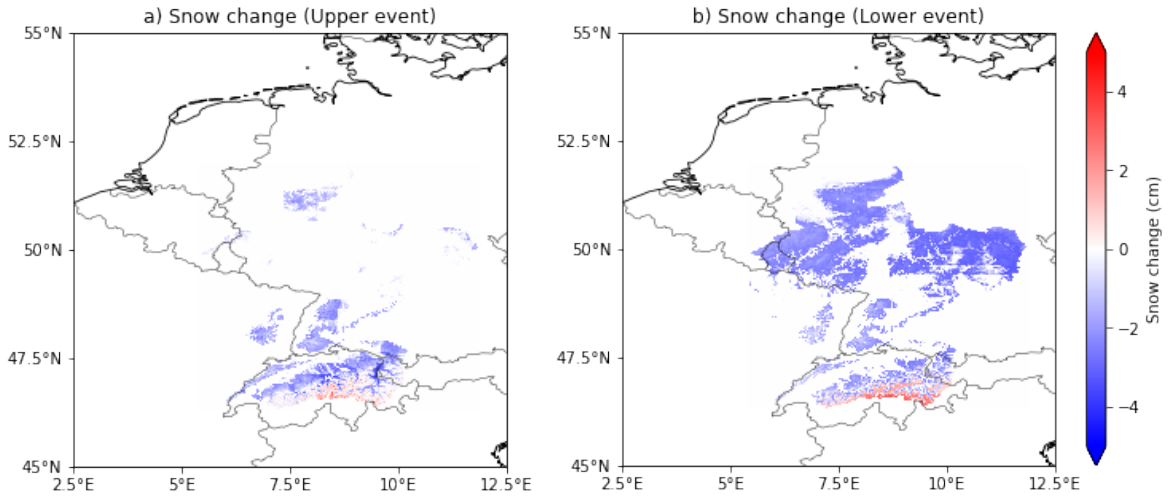

Figure 15: The change of the snow layer after the events compared to before the events simulated in the increased snow run.

The evolution of the mean groundwater storage in figure 16 showed an expected increase after the precipitation events for all runs. The increased snow run started with the same storage as the base run, but the groundwater storage increased more along the run due to the supply of melting water from the additional snow. In contrast with the snow simulations in figure 14, the increased storage runs started to converge already directly after the occurrence of the events. The differences between the runs disappeared during the second storage peak in both events halfway January. This could be explained by soil saturation occurring in all runs. Lastly, the second storage peaks corresponded with the timing of discharge peaks in Lobith (figure 13b,d) for both events.

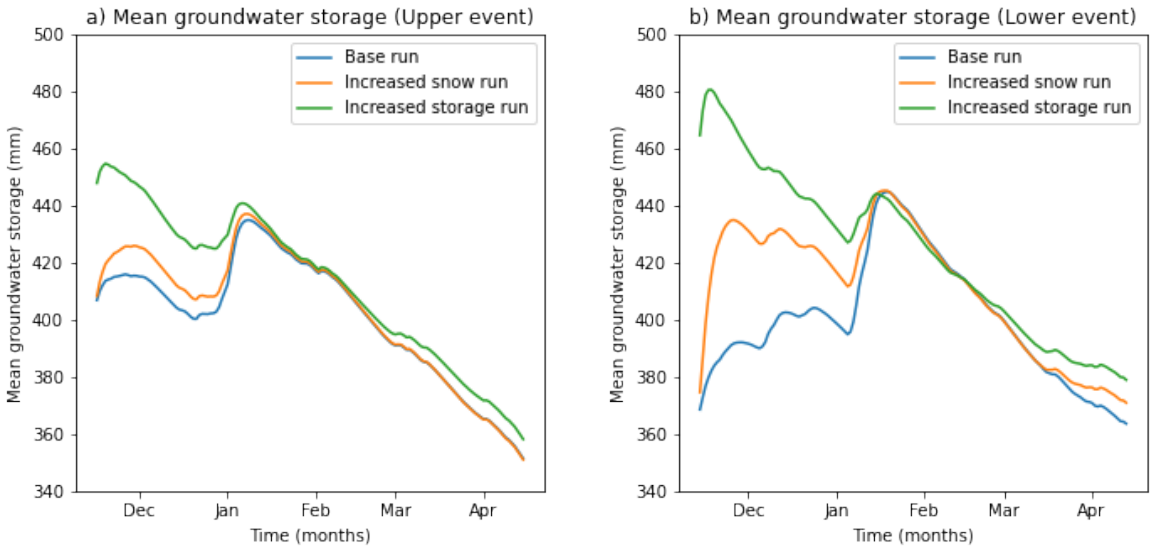

Figure 16: The evolution of the mean groundwater storage in the Rhine catchment in the base run, the increased snow run and the increased storage run for both events.

5 Discussion

In our study we found a significant increase of yearly AR occurrence and intensity from 1950-2020 and this was expected given the intensification of the hydrologic cycle (Allan et al., 2014; Lavers et al., 2013; Hill et al., 2018). With global warming, more moisture is taken up into the atmosphere as could be derived from the Clausius-Clapeyron equation (Allan et al., 2014). Aside from moisture, high IVT values could also potentially be caused by an increase in wind speeds, but less is known about this component.

Surprisingly, no significant increase was found in the yearly total precipitation and extreme precipitation. Other studies, like Kew et al. (2011) used a global climate model and projected a 10% increase in 99th percentile precipitation sums for the winters of 2071-2100 in the Rhine catchment. The difference in significance could be caused by the shorter time range used in our studies and the selection of years exclusively in the past, with less visible effects of climate change compared to future projections. Frei et al. (2000) and Menzel et al. (2006) confirm the potential increase of (extreme) precipitation in the future, but express the large uncertainty range.

As expected, most ARs were detected in the western and northwestern boundaries of the Rhine catchment. ARs occur 16% of the time in the west and about 10% in the east. This finding is in line with Gimeno et al. (2016) stating that ARs occur not only along the Atlantic ocean, but also in areas up to Poland. In contrast, very little amounts of ARs occur in the Alpine part of the catchment, with ARs occurring locally only 2% of the time. Reason for this low percentage could be orographic enhancement, triggering rainfall. In that case, moisture is removed from the air and IVT values mostly stay below the threshold of AR-detection in mountainous areas.

Orographic enhancement is probably also the driver of the relatively high extreme precipitation values in the Alps. Furthermore, the link between IVT and extreme daily precipitation was stronger compared to areas with less orography. However, more extreme precipitation days were linked with ARs in the Lower Rhine than in the Upper Rhine because the IVT threshold for AR-detection was rarely met there. Even though few ARs were detected over the Alps, they may still be responsible for extreme precipitation in this region.

Obviously, the amount of detected ARs heavily depends on the detection method. A uniform IVT-threshold of 250 kg m^{-1} s^{-1} was used here, while other studies applied regional thresholds defined by local IVT percentiles. For example Guan and Waliser (2019) applied a combination of the 85th IVT percentile combined with a fixed minimum IVT value. Moreover, Rutz et al. (2019) made an overview of detection methods and distinguished between less and more restrictive methods with different IVT magnitudes and requirements on specific geometries. With a flexible method, more ARs could be detected in the Alps than in our study and more extreme precipitation in orographic regions would be associated with ARs.

Important disadvantage of our methods are the unequal sizes of the defined Upper and Lower Rhine areas. All precipitation is classified as AR-related if an AR is present somewhere in the area of interest. Therefore, precipitation in the relatively large Lower Rhine area is more likely to be considered "AR-related" false positively. Nevertheless, an intuitive border between both areas was chosen based on the AR climatology. A relative uniform distribution of AR occurrences was found in the Lower Rhine, whereas a strong decreasing gradient to the southeast was found within the Upper Rhine catchment (figure 7b). Moreover, the location of Basel is located at a natural border of two subcatchments and long timeseries of river discharge were available there. These arguments were considered more important than having two equally sized areas.

Compared to other studies we found relatively high local IVT values in the middle of ARs. In figure 3b of Ionita et al. (2020) an IVT of 800 kg m^{-1} s^{-1} were shown in the middle of the AR based on 20th Century Reanalysis data V3, while we found values 1100 kg m^{-1} s^{-1} at the same time and place with ERA5 data. The higher values in ERA5 could be explained be the high resolution of 0.25°x0.25° compared to 1°x1° resolution in 20CRv3. This high resolution raises the opportunity for more accurate calculations of extreme IVT values.

Lastly, the increased snow and storage runs after both selected precipitation events generally reached way higher discharge levels than the base runs. Extreme example was the discharge of 30000 m^3 s^{-1} in Lobith, which was four times higher than the base run and twice the level upon which levees in the Netherlands are constructed. Of course, these values are not realistic given the manually altered initial conditions and general overestimation of discharge peaks by wflow_sbm. However, these outcomes illustrated the strong discharge sensitivity to snow and groundwater conditions preceding AR-related precipitation events.

6 Conclusion

New finding of this study was the increase of AR occurrence and intensity over time in the Rhine catchment. This is mainly explained by an increase of the specific humidity component of the IVT, but more research could determine the role of the wind component. Even though we did not find a significant increase in (extreme) precipitation over the past 70 years, this is not unlikely to be found in the future given projections by other studies. Thus it is important to keep monitoring precipitation trends in the coming decades.

Secondly, ARs were rarely detected in the Alpine part of the Rhine catchment with a uniform IVT threshold of 250 kg m^{-1} s^{-1}. However, extreme precipitation was clearly linked with local extreme IVT values despite the relatively low values compared to other regions. For that reason, research on extreme precipitation in areas with high topography are recommended to use a flexible AR-detection method with an IVT threshold depending on local IVT extremes. By doing so, more ARs would be detected in these areas and the link between IVT and precipitation would be more pronounced.

Thirdly, vulnerability to Rhine river floods strongly depends on water storage preceding extreme precipitation events. This means that not only the extremeness of precipitation is relevant, but also its timing. As a rapid follow-up of events results in a high build-up of water storage in the form of groundwater or snow, we recommend to study the link between consecutive events and discharge peaks further. Additionally, a good focus of following research could be on variation of ARs and precipitation within years, for example per month or week.

7 Acknowledgement

I would like to thank Imme Benedict, my main supervisor, for her enthusiasm and useful advice. Also thanks to my second supervisor Albrecht Weerts, who introduced me to the hydrological model. In addition, I would like to express my appreciation to the participants of the thesis ring for providing clear and useful feedback on preliminary texts. Lastly, I would like to thank Karianne Ødemark for the script that helped my with the detection of ARs.

References

L. Alfieri, P. Burek, L. Feyen, and G. Forzieri. Global warming increases the frequency of river floods in Europe. *Hydrology and Earth System Sciences*, 19(5):2247–2260, 2015. ISSN 16077938. doi: 10.5194/hess-19-2247-2015.

R. P. Allan, C. Liu, M. Zahn, D. A. Lavers, E. Koukouvagias, and A. Bodas-Salcedo. Physically Consistent Responses of the Global Atmospheric Hydrological Cycle in Models and Observations. *Surveys in Geophysics*, 35(3):533–552, 2014. ISSN 01693298. doi: 10.1007/s10712-012-9213-z.

BAFU. Hochwasserwahrscheinlichkeiten Rhein - Basel. page 2, 2017. URL https://www.hydrodaten.admin.ch/lhg/sdi/hq_studien/hq_statistics/2289hq.pdf.

I. Benedict, K. Ødemark, T. Nipen, and R. Moore. Large-scale flow patterns associated with extreme precipitation and atmospheric rivers over Norway. *Monthly Weather Review*, 147(4): 1415–1428, 2019. ISSN 15200493. doi: 10.1175/MWR-D-18-0362.1.

G. Blöschl, L. Gaál, J. Hall, A. Kiss, J. Komma, T. Nester, J. Parajka, R. A. P. Perdigão, L. Plavcová, M. Rogger, J. L. Salinas, and A. Viglione. Increasing river floods: fiction or reality? *Wiley Interdisciplinary Reviews: Water*, 2(4):329–344, 2015. doi: 10.1002/wat2.1079.

M. Cooper. Advanced Bash-Scripting Guide An in-depth exploration of the art of shell scripting Table of Contents. *Okt 2005 Abrufbar uber httpwww tldp orgLDPabsabsguide pdf Zugriff 1112 2005*, 2274(November 2008):2267–2274, 2010. ISSN 08856087. doi: 10.1002/hyp. URL http://jamsb.austms.org.au/courses/CSC2408/semester3/resources/ldp/abs-guide.pdf.

DWD. DWD. 2020. URL https://www.dwd.de/DE/leistungen/klimadatendeutschland/mittelwerte/nieder_8110_fest_html.html?view=nasPublication&nn=16102.

C. Frei, H. Davies, J. Gurtz, and C. Schär. Climate dynamics and extreme precipitation and flood events in Central Europe. *Integrated Assessment*, 1(4):281–300, 2000. ISSN 1389-5176. doi: 10.1023/A:1018983226334.

L. Gimeno, F. Dominguez, R. Nieto, R. Trigo, A. Drumond, C. J. Reason, A. S. Taschetto, A. M. Ramos, R. Kumar, and J. Marengo. Major Mechanisms of Atmospheric Moisture Transport and Their Role in Extreme Precipitation Events. *Annual Review of Environment and Resources*, 41:117–141, 2016. ISSN 15435938. doi: 10.1146/annurev-environ-110615-085558.

B. Guan and D. E. Waliser. Tracking Atmospheric Rivers Globally: Spatial Distributions and Temporal Evolution of Life Cycle Characteristics. *Journal of Geophysical Research: Atmospheres*, 124(23):12523–12552, 2019. ISSN 21698996. doi: 10.1029/2019JD031205.

H. Hersbach, B. Bell, P. Berrisford, S. Hirahara, A. Horányi, J. Muñoz-Sabater, J. Nicolas, C. Peubey, R. Radu, D. Schepers, A. Simmons, C. Soci, S. Abdalla, X. Abellan, G. Balsamo, P. Bechtold, G. Biavati, J. Bidlot, M. Bonavita, G. De Chiara, P. Dahlgren, D. Dee, M. Diamantakis, R. Dragani, J. Flemming, R. Forbes, M. Fuentes, A. Geer, L. Haimberger, S. Healy, R. J. Hogan, E. Hólm, M. Janisková, S. Keeley, P. Laloyaux, P. Lopez, C. Lupu, G. Radnoti, P. de Rosnay, I. Rozum, F. Vamborg, S. Villaume, and J. N. Thépaut. The ERA5 global reanalysis. *Quarterly Journal of the Royal Meteorological Society*, 146(730):1999–2049, 2020. ISSN 1477870X. doi: 10.1002/qj.3803.

S. A. Hill, Y. Ming, and M. Zhao. Robust responses of the Sahelian hydrological cycle to global warming. *Journal of Climate*, 31(24):9793–9814, 2018. ISSN 08948755. doi: 10.1175/JCLI-D-18-0238.1.

R. O. Imhoff, W. J. van Verseveld, B. van Osnabrugge, and A. H. Weerts. Scaling Point-Scale (Pedo)transfer Functions to Seamless Large-Domain Parameter Estimates for High-Resolution Distributed Hydrologic Modeling: An Example for the Rhine River. *Water Resources Research*, 56(4):1–28, 2020. ISSN 19447973. doi: 10.1029/2019WR026807.

M. Ionita, V. Nagavciuc, and B. Guan. Rivers in the sky, flooding on the ground. *Hydrology and Earth System Sciences Discussions*, (April):1–28, 2020. ISSN 1812-2108. doi: 10.5194/hess-2020-149.

S. F. Kew, F. M. Selten, G. Lenderink, and W. Hazeleger. Robust assessment of future changes in extreme precipitation over the Rhine basin using a GCM. *Hydrology and Earth System Sciences*, 15(4):1157–1166, 2011. ISSN 10275606. doi: 10.5194/hess-15-1157-2011.

KNMI. https://www.knmi.nl, 2020.

D. A. Lavers, R. P. Allan, E. F. Wood, G. Villarini, D. J. Brayshaw, and A. J. Wade. Winter floods in Britain are connected to atmospheric rivers. *Geophysical Research Letters*, 38(23): 1–8, 2011. ISSN 00948276. doi: 10.1029/2011GL049783.

D. A. Lavers, R. P. Allan, G. Villarini, B. Lloyd-Hughes, D. J. Brayshaw, and A. J. Wade. Future changes in atmospheric rivers and their implications for winter flooding in Britain. *Environmental Research Letters*, 8(3), 2013. ISSN 17489326. doi: 10.1088/1748-9326/8/3/034010.

M. Lu, U. Lall, A. Schwartz, and H. Kwon. Precipitation predictability associated with tropical moisture exports and circulation patterns for a major flood in France in 1995. *Water Resources Research*, 49(10):6381–6392, 2013. ISSN 00431397. doi: 10.1002/wrcr.20512.

L. Menzel, A. H. Thieken, D. Schwandt, and G. Bürger. Impact of climate change on the regional hydrology - Scenario-based modelling studies in the German Rhine catchment. *Natural Hazards*, 38(1-2):45–61, 2006. ISSN 0921030X. doi: 10.1007/s11069-005-8599-z.

H. Paltan, D. Waliser, W. H. Lim, B. Guan, D. Yamazaki, R. Pant, and S. Dadson. Global Floods and Water Availability Driven by Atmospheric Rivers. *Geophysical Research Letters*, 44(20):387–10, 2017. ISSN 19448007. doi: 10.1002/2017GL074882.

F. M. Ralph and M. D. Dettinger. Historical and national perspectives on extreme west coast precipitation associated with atmospheric rivers during december 2010. *Bulletin of the American Meteorological Society*, 93(6):783–790, 2012. ISSN 00030007. doi: 10.1175/BAMS-D-11-00188.1.

A. M. Ramos, R. M. Trigo, M. L. Liberato, and R. Tomé. Daily precipitation extreme events in the Iberian Peninsula and its association with atmospheric rivers. *Journal of Hydrometeorology*, 16(2):579–597, 2015. ISSN 15257541. doi: 10.1175/JHM-D-14-0103.1.

J. J. Rutz, W. James Steenburgh, and F. Martin Ralph. Climatological characteristics of atmospheric rivers and their inland penetration over the western united states. *Monthly Weather Review*, 142(2):905–921, 2014. ISSN 00270644. doi: 10.1175/MWR-D-13-00168.1.

J. J. Rutz, C. A. Shields, J. M. Lora, A. E. Payne, B. Guan, P. Ullrich, T. O'Brien, L. R. Leung, F. M. Ralph, M. Wehner, S. Brands, A. Collow, N. Goldenson, I. Gorodetskaya, H. Griffith, K. Kashinath, B. Kawzenuk, H. Krishnan, V. Kurlin, D. Lavers, G. Magnusdottir, K. Mahoney, E. McClenny, G. Muszynski, P. D. Nguyen, M. Prabhat, Y. Qian, A. M. Ramos, C. Sarangi, S. Sellars, T. Shulgina, R. Tome, D. Waliser, D. Walton, G. Wick, A. M. Wilson, and M. Viale. The Atmospheric River Tracking Method Intercomparison Project (ARTMIP): Quantifying Uncertainties in Atmospheric River Climatology. *Journal of Geophysical Research: Atmospheres*, 124(24):13777–13802, 2019. ISSN 21698996. doi: 10.1029/2019JD030936.

A. Stohl, C. Forster, and H. Sodemann. Remote sources of water vapor forming precipitation on the Norwegian west coast at 60°N - A tale of hurricanes and an atmospheric river. *Journal of Geophysical Research Atmospheres*, 113(5):1–13, 2008. ISSN 01480227. doi: 10.1029/2007JD009006.

A. H. Te Linde, P. Bubeck, J. E. Dekkers, H. De Moel, and J. C. Aerts. Future flood risk estimates along the river Rhine. *Natural Hazards and Earth System Science*, 11(2):459–473, 2011. ISSN 15618633. doi: 10.5194/nhess-11-459-2011.